crystals

MDPI

Article

Wear Behaviour of Graphene-Reinforced Ti-Cu Waste-Metal Friction Composites Fabricated with Spark Plasma Sintering

Mária Podobová, Viktor Puchý, Richard Sedlák *, Dávid Medveď, Róbert Džunda and František Kromka

Institute of Materials Research SAS, Watsonova 47, 04001 Košice, Slovakia; mpodobova@saske.sk (M.P.); vpuchy@saske.sk (V.P.); dmedved@saske.sk (D.M.); rdzunda@saske.sk (R.D.); fkromka@saske.sk (F.K.)
* Correspondence: rsedlak@saske.sk; Tel.: +421-55-792-2400

Abstract: In this study, we fabricated Ti-Cu-based friction composites containing waste-metal (Ti, CuZn, stainless steel (SSt), MgAl), Al_2O_3 due to improving properties and its good compatibility with copper and graphene nanoplatelets as reinforcement and lubricant component, using planetary ball mill and technique based on Spark Plasma Sintering (SPS). Understanding the wear behaviour of such engineered friction composites is essential to improve their material design and safety, as these materials could have the potential for use in public and industrial transportation, such as high-speed rail trains and aircraft or cars. This is why our study is focused on wear behaviour during friction between function parts of devices. We investigated the composite materials designed by us in order to clarify their microstructural state and mechanical properties. Using different loading conditions, we determined the Coefficient of Friction (COF) using a ball-on-disc tribological test. We analysed the state of the samples after the mentioned test using a Scanning Electron Microscope (SEM), then Energy-Dispersive X-ray Spectroscopy (EDS), and confocal microscopy. Also, a comparative analysis of friction properties with previously studied materials was performed. The results showed that friction composites with different compositions, despite the same conditions of their compaction during sintering, can be defined by different wear characteristics. Our study can potentially have a significant contribution to the understanding of wear mechanisms of Ti-Cu-based composites with incorporated metal-waste and to improving their material design and performance. Also, it can give us information about the possibilities of reusing metal-waste from different machining operations.

Keywords: Ti-Cu based composites; graphene; metal-waste; sintering; wear; COF

check for updates

Citation: Podobová, M.; Puchý, V.; Sedlák, R.; Medveď, D.; Džunda, R.; Kromka, F. Wear Behaviour of Graphene-Reinforced Ti-Cu Waste-Metal Friction Composites Fabricated with Spark Plasma Sintering. *Crystals* **2024**, *14*, 948. https://doi.org/10.3390/cryst14110948

Academic Editor: Vladislav V. Kharton

Received: 9 October 2024
Revised: 24 October 2024
Accepted: 28 October 2024
Published: 31 October 2024

Copyright: © 2024 by the authors. Licensee MDPI, Basel, Switzerland. This article is an open access article distributed under the terms and conditions of the Creative Commons Attribution (CC BY) license (https://creativecommons.org/licenses/by/4.0/).

1. Introduction

Composites with a metal base are characterised by a base enriched with components such as metal, ceramic, or organic particles, which should result in improved properties such as thermal and electrical conductivity, resistance to corrosion and wear, hardness, mechanical strength, and also bacterial properties [1].

The material composition mainly consists of base metal, lubrication element, and friction element. Copper-based materials are usually tin, lead, and zinc alloys, possess such properties as good thermal conductivity, corrosion resistance, and good friction resistance [2–5], mainly used in "wet" clutches. Iron-based materials have a higher friction coefficient and heat resistance and are mostly used in dry, heavy-duty brakes. Usually, graphite and lead are used as lubrication components, sometimes molybdenum sulphide, copper sulphide, barium sulphide or boron nitride, and other solid lubricants are also used. The low melting point of lead, tin, etc. will melt partially at high temperatures, which can absorb friction heat and create a film on the contact surface to prevent bonding, seizing, and abrasion. Friction components are used to improve friction conditions of a material, i.e., to increase the resistance to sliding. The main ones are oxides (SiO_2, Al_2O_3, Cr_2O_3), carbides (SiC, B_4C), and minerals (asbestos, mullite, etc.) [6–10].

Titanium and copper-based composites have come into the spotlight in the last few decades due to their exceptional physical and mechanical properties. The wide range of their use covers many industries where friction components are used, components for special applications in extreme conditions, e.g., friction, energy transfer, chemical factories, refineries, aircraft, automotive, biomedical, etc.

By combining the previously mentioned components, new advanced materials with exceptional properties are created. Titanium itself has many excellent properties, such as strength, high modulus of elasticity, and resistance to both chemicals and heat, as well as to wear. Similarly, copper and its alloys, have various uses thanks to excellent physical, mechanical, and chemical properties, of which we emphasize high thermal conductivity and corrosion resistance [11].

But lightweight titanium (Ti) and pure copper (Cu) have limited use due to their limited friction and wear properties [12,13], especially at high loads, high/low temperatures, in vacuum (Ti), when used in aircraft components, automotive, engine parts, exhaust systems (Cu) [14–17].

To improve the friction and wear control of Ti alloys, soft lubricants like CuAg [18], CuSnZn [19], and SnAgCu [20–22] have been used. The result of the use of these soft materials is the creation of an interface that has the effect of reducing the coefficient of friction and wear. However, micro/nano cracks were formed at the interface due to weak load ability. Kang et al. [23] found, that for improving the tribological properties of titanium alloys, the addition of light-weighted MgAl is useful (low density 1.5–1.8 g/cm^3, low melting point approx. 443 °C, great shock absorption and ductility).

Various authors added different materials into the copper-based composites [24], for example, Nurmohammadi Omran et al. [25] determined tribological properties of the copper–graphene composite, resulting in delamination with increasing the accumulative roll bonding cycles. Wei et al. [26] used gas pressure sintering to develop a copper-graphite-TiC composite. Aluminium oxide (Al_2O_3) and nickel (Ni) with their good compatibility with copper result in complete solid solubility with copper, without the formation of separated phases or other chemical compounds [27–29]. The combination of Ni (local strengthening) and Al_2O_3 (reinforcement) enhances both the mechanical performance and electrical conductivity of copper composites or alloys [30,31]. Such alloying elements as Zinc (Zn), Silver (Ag), Magnesium (Mg), Aluminium (Al), Silicon (Si), Iron (Fe), Beryllium (Be), and Tin (Sn) can increase the performance of copper [32–34].

A wide range of used ingredients has an essential role in positively influencing properties of materials for friction applications such as thermal resistance, physical, mechanical, tribological, and other properties [35–37]. Ideal composite for friction applications should provide a high coefficient of friction and also good wear resistance and corrosion resistance during friction [3,38]. Nowadays, in several engineering fields, wide-use of composites based on metals such as Al, Fe, Ni, Cu, Zn, Ag, Mg, and Si [39]. mixed with ceramic particles such as TiC, Si_3N_4, TiO_2, Al_2O_3, SiC, and ZrO_2. Al_2O_3 has received attention due to its high melting temperature, wear resistance, corrosion resistance, hardness, and elastic modulus [40,41].

It is important to state that there is an increased interest in guaranteeing ecological and low-cost production. The sources of natural raw materials are being depleted and the requirements for environmental protection are the focus of interest for both manufacturers and scientists. One of the possible approaches is the use of waste materials, as additional components, from other production processes, for example from machining operations [42]. Metal waste usable for the production of metal-based composites, or metal-ceramic composites can be titanium, aluminium, copper, stainless steel (stainless steel scrubber sponges), MgAl, CuZn, etc. in the form of powders, fibres, chips, etc. of different particle sizes and shapes.

In previous experiments [43], composites with the addition of titanium waste in the form of fibres and chips (25, 40, 60 wt.%) into Cu-Fe base, with a mixture of ZrO_2, SiC, and graphene nanoplatelets were prepared by mixing in turbula and spark plasma

sintered and microstructure and tribological properties were determined. The optimal tribological behaviour has been observed for the "40 wt.% of Ti" composite. Further study has been carried out on microstructure and friction properties of metal–ceramic composites consisting of commercial powders mixed with waste metal powders and chips (MgAl, CuZn, and Al), with an amount of Ti chips 40 wt.% according to previous experiments [11]. The composites were prepared by mixing in turbula and sintered by SPS.

In this work, composites based on Ti-Cu with the addition of "waste materials" such as SSt, CuZn, MgAl, Al_2O_3, and graphene nanoplatelets (GNPs) prepared by SPS were studied. The main milestone of this work is to investigate the possibility of using selected metal "waste materials" by incorporating them into the Ti-Cu base, with the aim of preparing composites suitable for friction applications with regard to the required tribological properties and point out the possibilities for recycling these waste materials in materials for friction applications.

2. Experimental Materials and Methods

For experimental research, we prepared composites that are a combination of a Ti-Cu metal base (Ti-waste in the form of chips, Cu-waste powder), with the addition of Al_2O_3 ceramics and other selected waste metal materials in the form of powders and chips (CuZn, MgAl, stainless steel SSt-stainless steel wires, metal wire sponge). To improve friction conditions, we added 5 wt.% graphene. The exact composition of our three experimental composites in wt.% can be seen in Table 1.

Table 1. Composition of the experimental composites (wt.%).

Composite Components	TC1	TC2	TC3
Ti chips	40	40	40
Cu	25	25	25
Stainless steel (wire-SSt)	15	-	-
MgAl	-	15	-
CuZn	-	-	15
Al_2O_3	15	15	15
GNPs	5	5	5

TC1—40Ti-25Cu-15SSt-15Al_2O_3-5GNPs, TC2—40Ti-25Cu-15MgAl-15Al_2O_3-5GNPs, TC3—40Ti-25Cu-15CuZn-15Al_2O_3-5GNPs.

Three different mixtures of Ti-Cu-based metal composite materials were prepared through Spark Plasma Sintering (SPS). The experimental composites (Table 1) were designed with regard to their desired properties, e.g., suitable coefficient of friction, sufficient wear resistance, and reduced fading. The characterisation of raw (*) and waste (**) materials used to prepare experimental composites is given in Table 2.

Unsorted waste Ti-chips (purity: 98%, supplier: pkchemie—kovyachemie.cz, 2% of impurities may include Fe, Al, V, Ni, and oil from machining, variously sized and shaped chips), Stainless steel (Metal wire sponge/scourer, commonly available in stores), MgAl alloy—variously sized chips and shavings (supplier: pkchemie—kovyachemie.cz, Mg—89.5–91%, Al—7.5–9% + impurities up to 1% Zn, Mn, Cu), Cu powder (supplier: pkchemie—kovyachemie.cz, Cu powder > 98% + oil from machining, average grain size: 35 μm), CuZn powder (supplier: pkchemie—kovyachemie.cz, Cu powder > 70%, Zn powder stabilized < 30%, average grain size—35 μm), Al_2O_3 powder (supplier: Thermo Scientific Chemicals, ThermoFisher (Kandel) GmbH, Kandel, Germany, powder α-phase < 1.0 μm, 99.9% Al_2O_3), and graphene GNPs (synthetic, grain size: 20 μm, supplier: Sigma Aldrich) Schelldorf, Germany.

Table 2. Characterisation of raw (*) and waste (**) materials used for the preparation of investigated composites.

Material	Size and Form	Purity	Supplier
Ti (**)	variously sized and shaped chips	98% Ti, impurities: Fe, Al, V, Ni, and oil from machining	Pkchemie-kovyachemie.cz
Cu (**)	powder with 35 μm average grain size	min. 98% Cu, impurities: oil from machining	Pkchemie-kovyachemie.cz
Stainless steel (SSt) (*)	metal wire sponge (scourer)	approx. 88.20% Fe, 11.8% Cr, impurities from machining	commonly available in stores
MgAl (**)	variously sized chips and shavings	89.5–91% Mg, 7.5–9% Al, about 1% of impurities: Zn, Mn, Cu	Pkchemie-kovyachemie.cz
CuZn (**)	powder with 35 μm average grain size	Cu > 70%, Zn stabilised > 30%	Pkchemie-kovyachemie.cz
Al_2O_3 (*)	powder α-phase < 1.0 μm	99.9% Al_2O_3	Thermo Scientific Chemicals, ThermoFisher (Kandel) GmbH, Kandel, Germany
GNPs (*)	synthetic with 20 μm grain size	-	Sigma Aldrich

As shown in Figure 1, waste and raw metal components from different machining operations exhibit morphology of various sizes and shapes. Figure 1a represents waste Ti with variously sized and shaped chips, Figure 1b represents waste MgAl with irregular and variously sized and shaped chips and shavings, Figure 1c represents powder-like CuZn with an average particles size of 35 μm, Figure 1d shows powder-like Cu with the average particles size of 35 μm, and Figure 1e shows stainless steel scourer (metal wire sponge) (SSt) commonly available in stores. Each of the above-mentioned materials has its own specific influence on the resulting functional properties of the friction components. Since heat is generated during friction, the choice of correct and suitable materials is crucial. The heat generated during friction has a significant impact on the functional properties and at the same time the service life of components for friction applications. Therefore, the above-mentioned components were selected and combined concerning their potential to positively influence the friction properties and thus the service life of the experimental friction components designed by us. Titanium was used for its very good wear resistance as well as thermal and chemical resistance. The alloy based on Mg-Al with possible impurities is light and high-strength and provides better heat conduction. Copper is responsible for the increase in thermal conductivity. In addition to this, CuZn has very good corrosion resistance. In this way, it is possible to achieve more effective cooling of the friction components, as well as a significant improvement in their braking efficiency, which, therefore, directly affects the service life and functionality of such components. The optimal coefficient of friction (COF) of friction materials has to be 0.3–0.7 in dry friction conditions. Mixing metal components with Al_2O_3 ceramic powder has the task of improving hardness and cold friction conditions. On the other hand, thanks to graphene nanoplatelets (GNPs) acting as a lubricant, the level of friction is reduced by creating friction films. In addition, it also improves corrosion resistance and acts as an anti-noise agent on the contact friction surface.

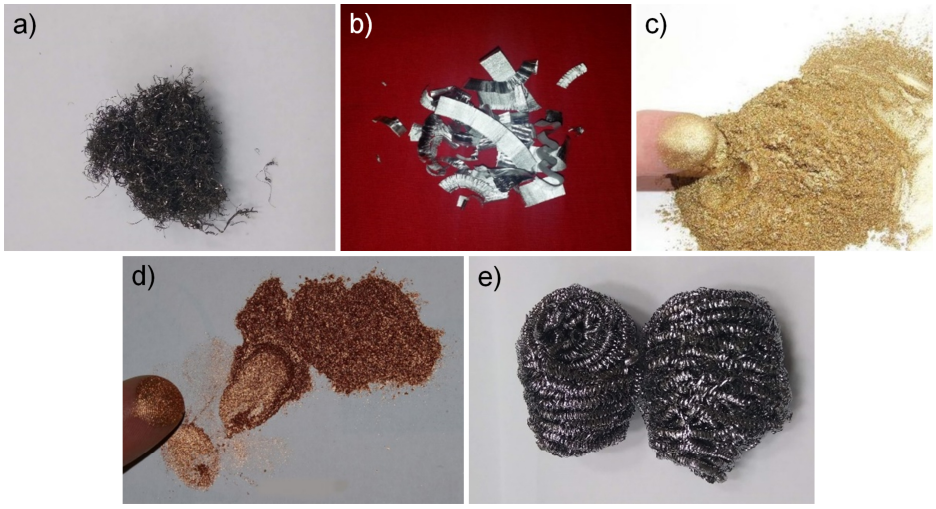

Figure 1. Morphologies of the four input waste materials: (**a**) Ti, (**b**) MgAl, (**c**) CuZn, (**d**) Cu, and (**e**) SSt stainless steel.

Before mixing with other components, Ti chips and stainless steel wire sponge were added, each separately, into the so-called UFO disc mill (WAB AG, Switzerland) for 2 × 5 min, for refinement.

Then the other components were added to the mixtures of investigated composites as stated in Table 1. Powder mixtures were high-energy ball-milled in a planetary ball mill RETSCH PM 100, parameters of ball-milling were 250 rpm, milling lasted 2 h, the ratio of the powder mixture and WC grinding balls was 5:1, and milling was carried out wet in ethanol. After high-energy ball milling the experimental powder mixtures were dried for 8 h period at 90 °C.

These milled experimental composite powders were layered into a graphite mold with an inner diameter of 20 mm. An SPS machine (HP D 10SD, FCT Systeme, Frankenblick, Germany) was used for sintering the experimental mixtures. The sintering took place at the following parameters—vacuum 5 Pa, pulsed DC electric current was applied with a pulse duration of 15 ms and a pause of 3 ms during all sintering attempts. The temperature was measured using a top pyrometer focused inside the hole in the punch at a distance of 4 mm from the sample. The mold and punch assembly was wrapped in graphite insulating foil and placed in the SPS. The powder was then heated under low vacuum conditions (10 Pa). The sintering temperature was 1000 °C, the heating rate was 100 °C.min^{-1}, the dwelling time was 10 min, and the applied pressure was 50 MPa. The composite samples were sintered in the form of disks with a diameter of 20 mm and a thickness of 4 mm. All compacted discs were ground and subsequently polished with a series of SiC sandpapers down to 3 μm. After these processes, they were polished with diamond paste to a smooth surface. The apparent density was measured as the ratio between the apparent volume and the dry mass of the prepared samples. The macro-hardness was determined by Vickers hardness under a load of 5 kg and 10 kg for 10 s per measurement. The microstructure of the sintered composites was analysed using a scanning electron microscope (SEM) (Tescan Vega-3 LMU, Brno, Czech Republic) equipped with an energy dispersive X-ray spectrometer (EDXS) (Bruker XFlash Detector 410-M, Billerica, MA, USA) for surface chemical composition analysis. Scanning electron microscopy (SEM, JEOL JSM-7000F, Nieuw-Vennep, The Netherlands) equipped with an energy dispersive spectrometric analysis system (EDS) was also used to investigate the microstructure and spot analysis of the elemental chemical composition. Friction and wear of the composites were studied using a tribometer (CSM Instruments HTT, Peseux, Switzerland) in the air at room temperature using the conventional ball-on-disc technique. The tribological partner for each tested material was a polished bearing steel ball with a diameter of 6 mm, corresponding to the material of the counterpart in real brake systems. The applied load was 5 N and 10 N, the

sliding speed was 100 mm/s, and the sliding distance was 500 m. The morphology of the worn surfaces and the wear mechanisms were analysed using a confocal 3D optical profiler (PLu neox, SENSOFAR, Barcelona, Spain). The chemical composition of composite samples prepared by SPS and the original recycled powder was determined by EDXS analysis. X-ray diffraction phase analysis (XRD) was performed with a diffractometer (Philips X'Pert pro, Panalytical P.V., Almelo, The Netherlands) using Cu-Ka radiation. An XRD machine in Bragg–Brentano geometry, as a source of X-ray radiation, was used as a Cu target, and for detection, an RTMS (Real Time Multiple Strip) X'Celerator detector was used. Measurement was performed at 20°–90° 2θ angle with step size of 0.03° and 30 s time per step.

3. Results and Discussion

3.1. Sintering Behaviour, Microstructure, Morphology and Components Distribution

Figure 2a–c shows the SEM-EDS mapping of three milled powder mixtures (TC1–TC3) used in friction composites, revealing uniform dispersion of the powders within the titanium-copper base. EDS analysis indicates that the blue particles represent titanium, while the green particles correspond to graphene nanoplatelets. Across all composite powder samples, the graphene nanoplatelets (GNPs) were evenly distributed throughout the base, indicating the potential formation of an electrically conductive network that could improve the sintering process.



Figure 2. (**a**–**c**) TC1–TC3 (from left to right) composite powder mixtures after planetary ball milling.

Figure 3a,b shows the sintering curves and punch displacement (shrinkage) plots for the TC1–TC3 friction composite materials, heated at a rate of 100 °C/min. Four distinct shrinkage regions were identified. In the first region, below 400 °C, no shrinkage was observed in any samples. Shrinkage started in the second region, between 400 °C and 1000 °C, likely due to particle rearrangement, plastic deformation of the metallic phase, liquid phase formation, plastic deformation of graphite foils, sintering, and reduced porosity. In the third region, a more pronounced displacement occurred as uniaxial pressure increased from 3 kN to 16 kN at 1000 °C. In the fourth region, during the dwell at 1000 °C, minimal displacement changes were observed, indicating full sample densification.

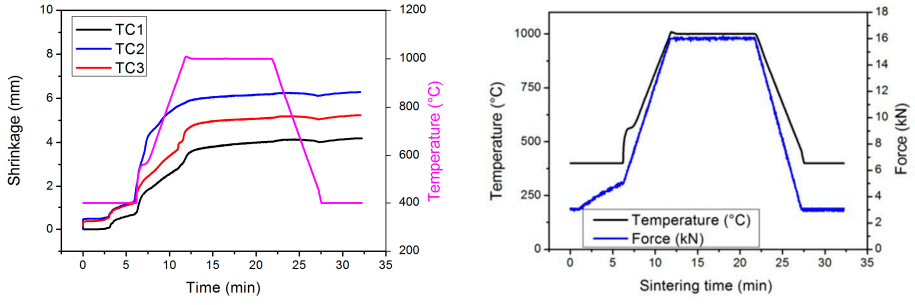

(**a**) (**b**)

Figure 3. (**a**,**b**) Sintering curves, shrinkage over time, and applied pressure force.

3.2. Tribological Behaviour

3.2.1. Coefficient of Friction

The friction and wear behaviour of the developed TC1–3 friction composites were assessed using a translational tribometer (Table 3). Figure 4 illustrates the variation in the coefficient of friction (COF) over time (seconds) for different loads (5 N, 10 N) at a sliding speed of 0.1 m/s. The dynamic friction coefficients of TC1–3 composites with a sliding force of 10 N are only slightly lower than those with a sliding force of 5 N. All composites indicate a similar COF between 0.4 and 0.6 under the increased loads. Figure 4 shows that the coefficient of friction (COF) exhibits periodic fluctuations over time due to the formation of a lubricating adhesive layer between the sample and the ball. As wear time progresses, this adhesive layer alternately disappears and re-forms, resulting in continuous variations in the COF. This is a beneficial characteristic, as a higher friction force can generate elevated local friction temperatures, indicating improved heat fade resistance in the developed brake composites that incorporate recycled materials (because the smaller friction force can create smaller local friction temperature this effect can lead to weaker or thinner friction film between friction pair). The run-in stage of the TC3 composite is slightly higher at both 5 and 10 N sliding forces. After 1000 sec sliding time at 5 N, the COF of TC3 composite crossed to stable wear stage with COF value circa 0.58, and at 10 N 0.55, respectively. The sample TC2 reported similar behaviour to TC3 at sliding force 5 N but at 10 N reported a lower COF probably due to a lower hardness value than TC3 which stabilises the creation of friction film. Friction composites should be engineered to achieve a range of performance characteristics, including a stable and moderate coefficient of friction (COF), a low wear rate, high recovery, minimal fade, and low sensitivity to changes in COF. Table 4 shows that COF strongly depends on the sort of third-added recycled component. At TC1 composite COF was 0.56 and 0.49 at 5 and 10 N normal load, respectively, with stainless steel as recycled additive. This was very similar to at TC3, COF 0.55 and 0.54 at 5 and 10 N normal load, respectively, with CuZn as a recycled additive. On the contrary, sample TC2 has COF 0.69 and 0.49 at 5 and 10 N normal load, respectively, with MgAl as a recycled additive. The TC2 sample at a lower load of 5 N shows the highest COF of 0.69 but at a higher load of 10 N COF was 0.49. This signalizes that composite containing MgAl as a recycled additive shows weaker fade resistance. Average friction coefficient values along with measurable deviations are displayed on the graph below, Figure 5, for the investigated samples under 5 N and 10 N loads.

Table 3. Macro hardness, apparent densities, and wear rates of the studied composites.

Sample	Hardness HV5 (GPa)	Hardness HV10 (GPa)	Apparent Density (g/cm^3)	Wear Rate $\times 10^{-6}$ (mm^3/N.m) at 5 N	Wear Rate $\times 10^{-6}$ (mm^3/N.m) at 10 N
TC1	7.08 ± 1.35	6.92 ± 1.45	5.140	1.31×10^{-6}	2.37×10^{-6}
TC2	7.19 ± 1.34	7.88 ± 1.87	4.523	0.70×10^{-6}	0.10×10^{-6}
TC3	9.15 ± 0.19	8.32 ± 0.63	4.526	0.27×10^{-6}	0.91×10^{-6}

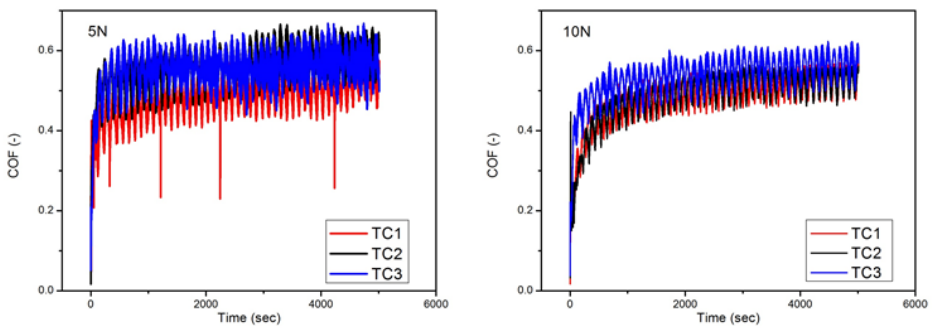

Figure 4. Coefficient of friction vs. time for different values of load (5 N, 10 N).

Table 4. Coefficient of friction with standard deviation values.

Sample/Load (N)	Average	SD
TC1		
5 N	0.5578	0.1570
10 N	0.4909	0.1459
TC2		
5 N	0.6891	0.1399
10 N	0.4854	0.1459
TC3		
5 N	0.5504	0.1942
10 N	0.5346	0.1763

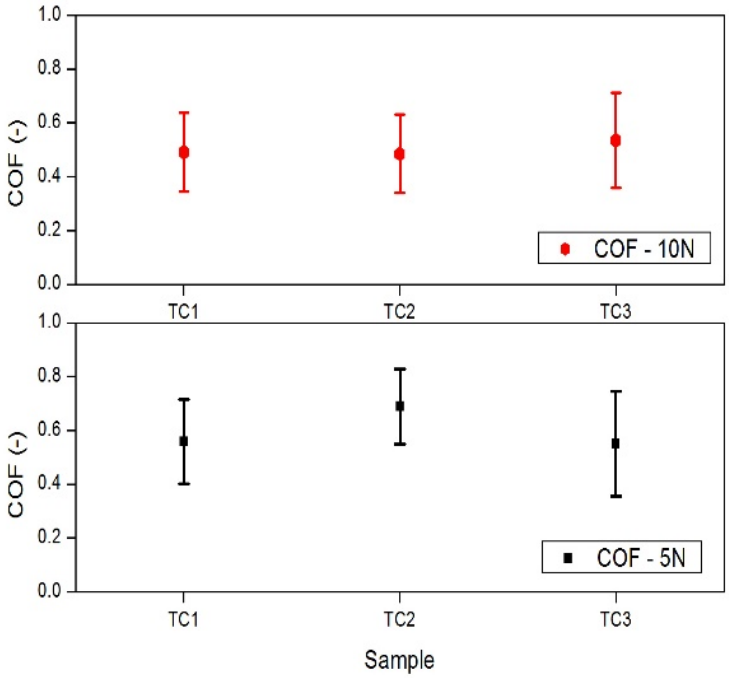

Figure 5. Average coefficient of friction for applied load 5N and 10N with deviation values.

3.2.2. Wear

Figure 6 shows their EDS mapping micrographs. The worn surfaces of the friction composites studied by SEM are shown in Figure 7. The strong features were observed in all micrographs. Figure 7a observed the thickness and discontinuity of the friction film, which is possibly caused by the enrichment of hard but brittle TiC phase, and therefore, a larger difference in hardness between phases can tend to destroy easily the oxidation film into debris [44]. Topographic changes on the friction surface during friction test can be related to intermetallic-ceramic phases interfacial adhesion failures, roughness changes, or non-uniformity properties such as thermal conductivity and residual stresses. The EDS elemental mapping image in Figure 6a in correlation with the morphology micrograph in Figure 7a–d shows some damage to the ingredients and the thinnest but discontinuous pieces of friction film enriched with Cu (Figure 7a), which was responsible for some wear. Due to the production of heat between friction pairs, the oxidation reactions occur between the debris and surface which resulted in the reduction in COF in the case of the TC1 composite more prominently than the TC2 and TC3.

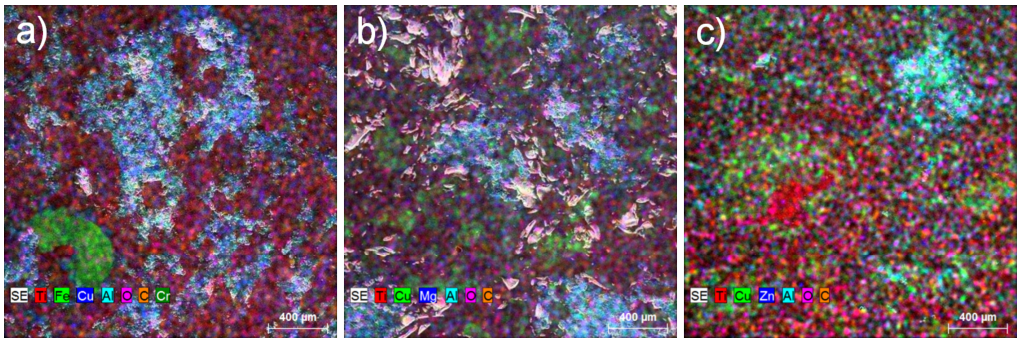

Figure 6. (**a**–**c**) SEM-EDX mapping TC1–TC3 area (**from left to right**).

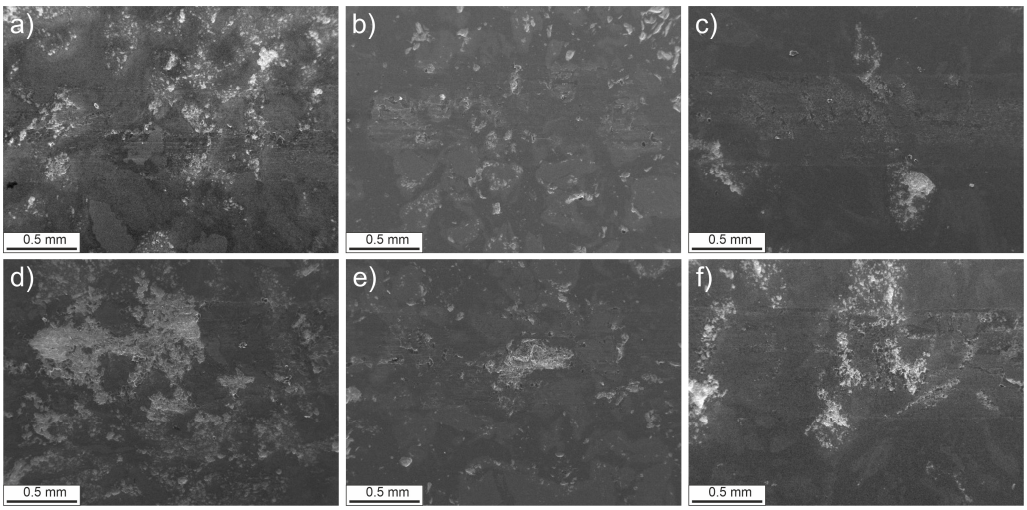

Figure 7. SEM from wear track TC1–TC3 (**from left to right**), (**a**–**c**) load 5 N, (**d**–**f**) load 10 N.

From Figure 8, it can be seen that the penetration depth and abraded volume of the TC3 friction composites containing CuZn are much lower than that containing SSt (TC1) and MgAl (TC2) under the same condition, indicating that the friction composites containing CuZn have a lower wear rate during the friction process. Recycled CuZn material is more suitable for the formation of friction film than SSt and MgAl and causes more uniform wear between friction pairs. At the composites with SSt and MgAl as recycled added material, it can be seen from Figure 8a,b that the friction surface demonstrates more depth friction track and more uneven wear. As the friction track depth increases, the groove action enhances and causes an increase in COF. Thus, the TC3 composite has the best friction properties.

3.3. XRD Analysis

Each sample was measured before and after sintering in order to evaluate the change of phase composition after SPS. Measured data were evaluated by program High Score (Malvern Panalytical, Almelo, The Netherlands) using a PDF-2 database for identification of phases. Figure 9 shows the results of the XRD analysis of the TC1–TC3 series of samples, comparing high-energy ball-milled powders and sintered discs. Results of XRD analysis suggest that during the SPS process, Ti and Cu form intermetallic phases identified as CuTi and Cu_3Ti. This can be determined in the TC1–TC3 samples series by the presence of peaks of lower intensity of Cu and Ti visible characteristic peaks; however, peaks matching intermetallic phases appear to be present after the SPS process which was also observed by [45,46]. In the TC1–TC3 series of samples, the presence of TiC was indicated after spark plasma sintering which was most likely formed after by reaction with graphene [47] supported by a relative decrease in graphene in sintered samples. The system contained a high amount of carbon originating from SPS graphite mold and dies. Thus, carbides

are forming, which is confirmed by the results from XRD and EDX analyses. In summary predominantly in the TC1–TC3 series of samples major phase change after SPS occurred by mixing/reacting of Cu and Ti resulting in identified CuTi and Cu_3Ti phases; however, there is a possibility that there is the presence of multiple stoichiometries Cu_xTi_y depended on the local concentration of elements.

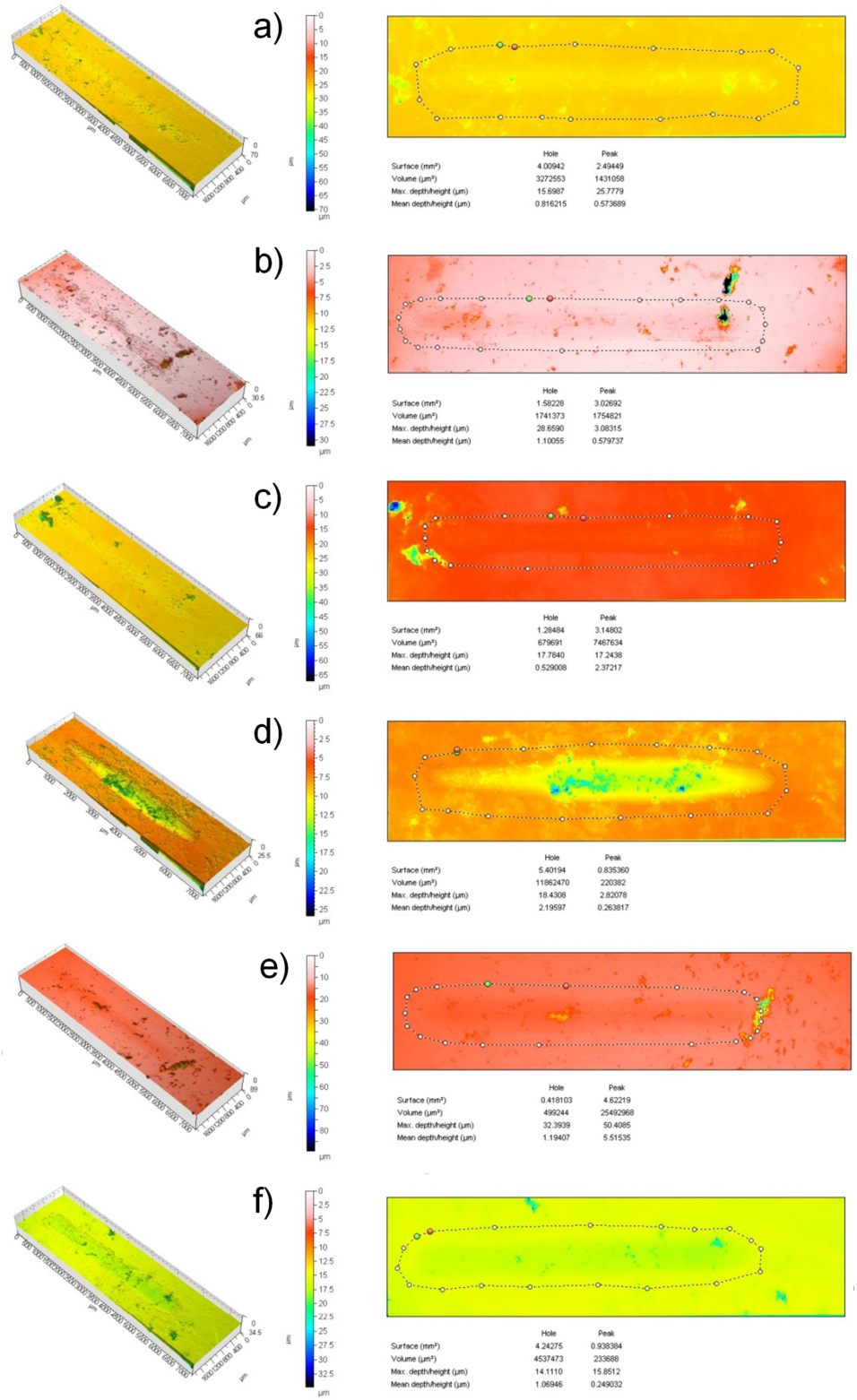

Figure 8. Visualisation of the confocal images of wear tracks (**a**–**c**) load 5 N, (**d**–**f**) load 10 N.

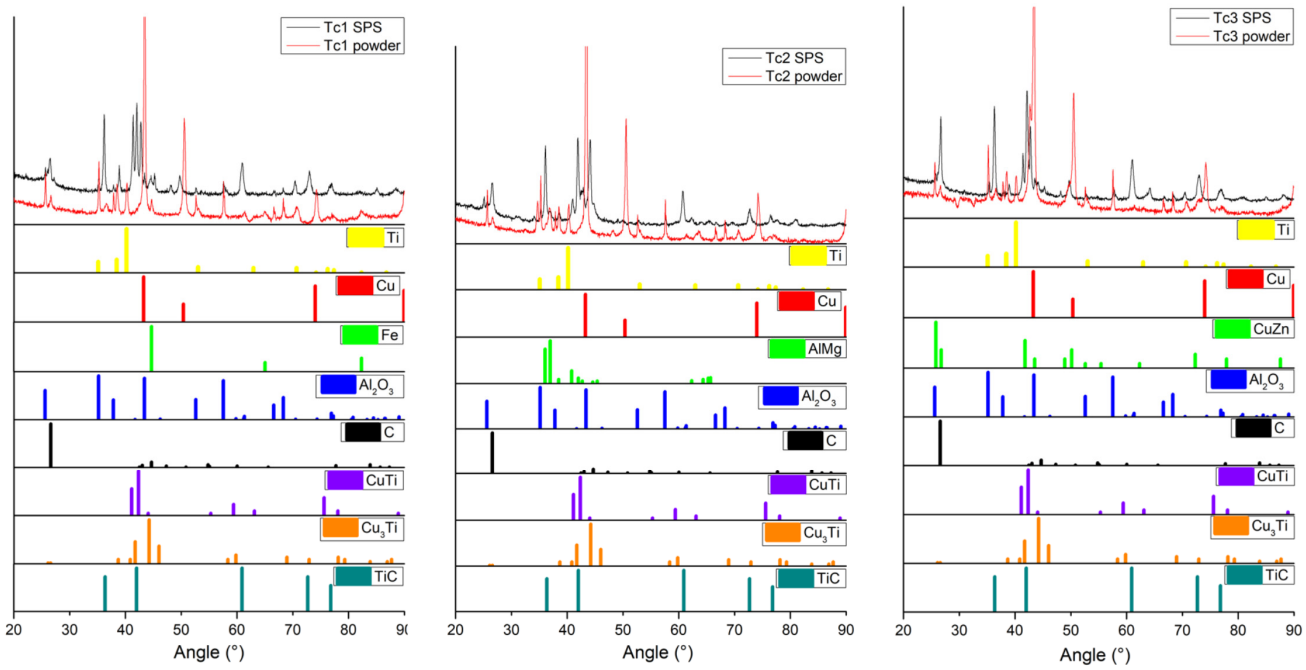

Figure 9. XRD records of samples TC1–TC3 (**from left to right**).

4. Conclusions

In this study, we fabricated Ti-Cu-based metal-ceramic friction composites with different waste metal powders and chips by SPS under sintering conditions (1000 °C, 50 MPa) in order to prepare composites with near to 100% density (non-porous) and subjected them to the ball-on-disc test under various loads (5 N and 10 N). Next, we performed surface and friction wear track analyses of the prepared composite samples using SEM, confocal microscopy, and XRD measurements. The following conclusions can be drawn based on the results obtained:

1. The Ti-Cu-based friction composites with different compositions fabricated with the SPS showed different relative densities and hardnesses, which varied with the addition of the third waste phase used. The base of the studied composites was Ti and Cu. It was chosen as a second phase in the ratio of 40 wt.% to 25 wt.%, taking into account the good results of previous experiments [11,43], where it was shown that this ratio had the most favourable effect on both COF and wear values.
2. Based on the used type of third added phases, the Ti-Cu-based friction composites exhibited different wear mechanisms. Sample TC1 and TC2 showed mainly abrasive wear with surface delamination, while sample TC3 showed both abrasive and adhesive wear with the creation of friction film. This is because the differences in the hardnesses and apparent densities of the samples affected the size and amount of debris produced during the wear test. During the tribological tests, a higher load resulted in a greater degree of oxidation. This is because a greater load generated more heat and it was accelerating the oxidation process and contributing to the formation of the oxide film. As a result, the samples with high oxidation wear exhibited lower COF values.
3. The friction test performed on the TC3 sample showed the best friction characteristics in this study. This was owing to the differences in the tribofilm formation mechanism and the COF stability during increasing load in the tribological tests in the TC3 sample. The COF value at 5 N and 10 N decreased from 0.56 to 0.49 in the TC1, from 0.69 to 0.49, and from 0.55 to 0.54 in the TC2 and TC3, respectively. It was confirmed that the friction test of Ti-Cu samples resulted in the same wear mechanism as at the Ti-Fe materials from our previous study [11,43].

4. The preparing conditions such as parameters of ball milling, sintering temperature, and pressure used during the sintering of friction composites have a determining effect on their friction and wear characteristics. In particular, in the case of the recycled powders of Ti-Cu-based friction composite materials, a temperature, and pressure of 1000 °C and 50 Mpa, respectively, would result in the best wear characteristics. Furthermore, the results of the wear mechanism analysis performed in this study can be helpful in the development of improved Ti-Cu-based recycled friction composite materials.
5. This study proves that the planetary ball milling and SPS sintering technique can be used to fabricate Ti-Cu-based waste metal friction composites. The Ti-Cu-CuZn-Al_2O_3-GNPs composites have better COF behaviour and wear resistance than those with MgAl and stainless steel metal additives.

Author Contributions: Conceptualization, V.P.; methodology, V.P. and M.P.; validation, V.P., M.P. and R.S.; formal analysis, V.P. and R.S.; investigation, V.P., D.M., R.D. and F.K.; data curation, V.P.; writing—original draft preparation, V.P. and M.P.; writing—review and editing, V.P., M.P. and R.S.; visualization, V.P.; supervision, V.P.; project administration, V.P., R.S.; funding acquisition, V.P., M.P. and R.S. All authors have read and agreed to the published version of the manuscript.

Funding: This research was supported by the Slovak Research and Development Agency, under contract: APVV-18-0438—acknowledged by V.P. The work was also supported by the Scientific Grant Agency of the Ministry of Education, Science, Research and Sport of the Slovak Republic and the Slovak Academy of Sciences, project: VEGA 2/0113/23—acknowledged by M.P. R.S. acknowledges the support: "Funded by the EU NextGenerationEU through the Recovery and Resilience Plan for Slovakia under the project No. 09I03-03-V04-00746".

Data Availability Statement: Data are contained within the article.

Conflicts of Interest: The authors declare no conflicts of interest. The funders had no role in the design of the study; in the collection, analyses, or interpretation of data; in the writing of the manuscript; or in the decision to publish the results.

References

1. Pingale, A.D.; Owhal, A.; Katarkar, A.S.; Belgamwar, S.U. Fabrication and tribo-mechanical performance of Cu@Al_2O_3 composite. *Mater. Today Proc.* **2022**, *64*, 1175–1181. [CrossRef]
2. Thankachan, T.; Prakash, K.S.; Kavimani, V. Investigating the effects of hybrid reinforcement particles on the microstructural, mechanical and tribological properties of friction stir processed copper surface composites. *Compos. Part B Eng.* **2019**, *174*, 107057. [CrossRef]
3. Peng, T.; Yan, Q.; Li, G.; Zhang, X.; Wen, Z.; Jin, X. The braking behaviors of Cu-based metallic brake pad for high-speed train under different initial braking speed. *Tribol. Lett.* **2017**, *65*, 135. [CrossRef]
4. Asif, M.; Chandra, K.; Misra, P.S. Development of iron based brake friction material by hot powder preform forging technique used for medium to heavy duty applications. *J. Min. Mater. Charact. Eng.* **2011**, *10*, 231–244. [CrossRef]
5. Liew, K.W.; Nirmal, U. Frictional performance evaluation of newly designed brake pad materials. *Mater Des.* **2013**, *48*, 25–33. [CrossRef]
6. Available online: https://www.chinagrtech.com/info/introduction-of-powder-metallurgy-friction-mat-90577681.html (accessed on 9 September 2024).
7. Bijwe, J. Multifunctionality of non-asbestos organic brake materials. *Multifunct. Polym. Compos. Chall. New Solut.* **2015**, 551–572. [CrossRef]
8. Song, J. Performance evaluation of a hybrid electric brake system with a sliding mode controller. *Mechatronics* **2005**, *15*, 339–358. [CrossRef]
9. Zhang, W. Tribology of SiC ceramics under lubrication: Features, developments and perspectives. *Curr. Opin. Solid State Mater. Sci.* **2022**, *26*, 101000. [CrossRef]
10. Zhang, W. A review of tribological properties for boron carbide ceramics. *Prog. Mater. Sci.* **2021**, *116*, 100718. [CrossRef]
11. Podobova, M.; Puchy, V.; Falat, L.; Dzunda, R.; Besterci, M. Waste metals based metal-matrix ceramic-reinforced composites for friction applications. *Met. Mater.* **2022**, *60*, 351–362. [CrossRef]
12. Xiao, N.; Yang, K.; Yin, X.; Zhang, F.; Wu, Y.; Zhang, H.; Xiong, B.; Zhu, Y.F.; Duan, M.; Zhang, C. Analysis of mechanical properties and tribological optimization of Ti-16 wt%Ni alloys with MgAl–Al_2O_3-graphene microchannels. *Wear* **2022**, *510–511*, 204515. [CrossRef]

13. Dwivedi, S.P.; Sharma, S. Development and characterization of Cu-Ni-Al_2O_3 surface composite developed by friction stir process technique. *Mater. Today Commun.* **2023**, *37*, 107399. [CrossRef]
14. Rominiyi, A.L.; Shongwe, M.B.; Jeje, S.O. Microstructure, tribological and oxidation behaviour of spark plasma sintered Ti-Ni-xTiCN composites. *J. Alloys Compd.* **2022**, *890*, 161857. [CrossRef]
15. Ranjan, S.; Mukherjee, B.; Islam, A. Microstructure, mechanical and high temperature tribological behaviour of graphene nanoplatelets reinforced plasma sprayed titanium nitride coating. *J. Eur. Ceram. Soc.* **2020**, *40*, 660–671. [CrossRef]
16. Yuan, S.; Toury, B.; Benayoun, S. Novel chemical process for preparing h-BN solid lubricant coatings on titanium-based substrates for high temperature tribological applications. *Surf. Coating. Technol.* **2015**, *272*, 366–372. [CrossRef]
17. Zhang, H.; Wen, Y.; Sha, X. Vacuum tribological properties and impact toughness of polycrystalline diamond based on titanium-coated diamond particle. *Diam. Relat. Mater.* **2020**, *103*, 107712. [CrossRef]
18. Hernan, D.; Mejia, V.; Perea, D.; Bejarano, G. Development and characterization of TiAlN (Ag, Cu) nanocomposite coatings deposited by DC magnetron sputtering for tribological applications. *Surf. Coating. Technol.* **2020**, *381*, 125095. [CrossRef]
19. Susilowati, S.E.; Fudholi, A.; Sumardiyanto, D. Mechanical and microstructural characteristics of Cu–Sn–Zn/Gr metal matrix composites processed by powder metallurgy for bearing materials. *Res. Eng.* **2022**, *14*, 100377. [CrossRef]
20. Xu, J.; Li, X.; Lu, J. An investigation into mechanics and tribology of SnAgCu and MoO_3 containing in 20CrMnTi based composites. *J. Alloys Compd.* **2020**, *831*, 154858. [CrossRef]
21. Bian, H.; Zhou, Y.; Song, X. Reactive wetting and interfacial characterization of ZrO_2 by SnAgCu-Ti alloy. *Ceram. Int.* **2019**, *45*, 6730–6737. [CrossRef]
22. Fu, W.; Hu, S.P.; Song, X.G.; Li, J.X.; Cao, J.; Feng, J.C.; Wang, G.D. Wettability and bonding of graphite by Sn0.3Ag0.7Cu-Ti alloys. *Carbon* **2017**, *121*, 536–543. [CrossRef]
23. Kang, Y.; Ma, H.; Wang, L. Analysis of self-regulating tribological functions of the MgAl microchannels prepared in the Ti alloys. *Tribol. Int.* **2021**, *154*, 106717. [CrossRef]
24. Sarmadi, H.; Kokabi, A.H.; Seyed Reihani, S.M. Friction and wear performance of copper–graphite surface composites fabricated by friction stir processing (FSP). *Wear* **2013**, *304*, 1–12. [CrossRef]
25. Omran, H.N.; Eivani, A.R.; Farbakhti, M.; Jafarian, H.R. Tribological properties of copper-graphene (CuG) composite fabricated by accumulative roll bonding. *J. Mater. Res. Technol.* **2023**, *25*, 4650–4657. [CrossRef]
26. Wei, H.; Feng, G.; Li, X.; Zhan, W.; Li, F.; Dai, Y.; Zou, J. Copper-graphite-TiC composites-synthesis and microstructure investigation. *Mater. Lett.* **2023**, *351*, 135005. [CrossRef]
27. Saxena, A.; Dwivedi, S.P.; Kaushik, A.; Sharma, S. Investigation on mechanical properties of ZTA+ Cr_3C_2 + Ni reinforced EN31 steel-based composite material: Micromechanical finite-element analysis. *Proc. Inst. Mech. Eng. Part E J. Process Mech. Eng.* **2022**, *237*, 1378–1393. [CrossRef]
28. Kumar, K.B.; Ingole, S.B.; Saeedjassim, A.; Gori, Y.; Kaushik, A.; Kumar, D.; Jain, A. Aluminum-foam by powder metallurgy: A review. *Mater. Today Proc.* **2023**. [CrossRef]
29. Sambasivam, S.; Gupta, N.; Jassim, A.S.; Singh, D.P.; Kumar, S.; Giri, J.M.; Gupta, M. A review paper of FSW on dissimilar materials using aluminum. *Mater. Today Proc.* **2023**. [CrossRef]
30. Dwivedi, S.P. Development and characterization of grinding sludge-reinforced aluminum-based composite by friction stir process technique. *World J. Eng.* **2023**, *21*, 924–932. [CrossRef]
31. Dwivedi, S.P.; Sharma, S.; Li, C.; Zhang, Y.; Kumar, A.; Singh, R.; Eldin, S.M.; Abbas, M. Effect of nano-TiO_2 particles addition on dissimilar AA2024 and AA2014 based composite developed by friction stir process technique. *J. Mater. Res. Technol.* **2023**, *26*, 1872–1881. [CrossRef]
32. Pingale, A.D.; Belgamwar, S.U.; Rathore, J.S. Synthesis and characterization of Cu–Ni/Gr nanocomposite coatings by electro-co-deposition method: Effect of current density. *Bull. Mater. Sci.* **2020**, *43*, 66, Electronic ISSN 0973-7669. [CrossRef]
33. Pingale, A.D.; Belgamwar, S.U.; Rathore, J.S. A novel approach for facile synthesis of Cu-Ni/GNPs composites with excellent mechanical and tribological properties. *Mater. Sci. Eng. B* **2020**, *260*, 114643. [CrossRef]
34. Pingale, A.D.; Belgamwar, S.U.; Rathore, J.S. Effect of graphene nanoplatelets addition on the mechanical, tribological and corrosion properties of Cu–Ni/Gr nanocomposite coatings by electro-co-deposition method. *Trans. Indian Inst. Met.* **2020**, *73*, 99–107. [CrossRef]
35. Shen, X.J.; Pei, X.Q.; Liu, Y.; Fu, S.Y. Tribological performance of carbon nanotube–graphene oxide hybrid/epoxy composites. *Compos. Part B-Eng.* **2014**, *57*, 120–125. [CrossRef]
36. Ma, Y.; Liu, Y.; Ma, S.; Wang, H.; Gao, Z.; Sun, J.; Tong, J.; Guo, L. Friction and wear properties of dumbbell-shaped jute fiber-reinforced friction materials. *J. Appl. Polym. Sci.* **2014**, *131*, 40748. [CrossRef]
37. Liu, Y.; Ma, Y.; Lv, X.; Yu, J.; Zhuang, J.; Tong, J. Mineral fibre reinforced friction composites: Effect of rockwool fibre on mechanical and tribological behaviour. *Mater. Res. Express* **2018**, *5*, 95308. [CrossRef]
38. Uyyuru, R.K.; Surappa, M.K.; Brusethaug, S. Tribological behavior of Al-Si-SiCp composites/automobile brake pad system under dry sliding conditions. *Tribol. Int.* **2007**, *40*, 365–373. [CrossRef]
39. Karuppasamy, K.; Ranganathan, B.; Rajendran, S. Evaluating the mechanical and tribological characteristics of aluminium hybrid composites incorporating ZrO_2 and graphite micro-particles. *Met. Mater.* **2024**, *62*, 101–109. [CrossRef]
40. Cheng, H.-C.; Chen, Y.-Y.; Chang, T.-L.; Chen, P.-H. Effect of biomimetic fishbonepatterned copper tubes on pool boiling heat transfer. *Int. J. Heat Mass Transf.* **2020**, *162*, 120371. [CrossRef]

41. Alizadeh, M.; Safaei, H. Characterization of Ni-Cu matrix, Al_2O_3 reinforced nano-composite coatings prepared by electrodeposition. *Appl. Surf. Sci.* **2018**, *456*, 195–203. [CrossRef]
42. Zhang, P.; Zhang, L.; Fu, K.; Cao, J.; Shijia, C.; Qu, X. Effects of different forms of Fe powder additives on the simulated braking performance of Cu-based friction materials for high-speed railway trains. *Wear* **2018**, *414–415*, 317–326. [CrossRef]
43. Podobová, M.; Puchý, V.; Falat, L.; Džunda, R.; Besterci, M.; Hvizdoš, P. Microstructure and Tribological behavior of SPS processed Fe/Ti-15wt.% Cu-based metal matrix composites with Incorporated waste Ti-chips. *Met. Mater.* **2020**, *58*, 83–91. [CrossRef]
44. Xiao, X.; Yin, Y.; Bao, J.; Lu, L.; Feng, X. Review on the friction and wear of brake materials. *Adv. Mech. Eng.* **2016**, *8*, 1687814016647300. [CrossRef]
45. Shichalin, O.O.; Sakhnevich, V.N.; Buravlev, I.Y.; Lembikov, A.O.; Buravleva, A.A.; Azon, S.A.; Yarusova, S.B.; Danilova, S.N.; Fedorets, A.N.; Belov, A.A.; et al. Synthesis of Ti-Cu multiphase alloy by spark plasma sintering: Mechanical and corrosion properties. *Metals* **2022**, *12*, 1089. [CrossRef]
46. Dong, R.; Zhu, W.; Zhao, C.; Zhang, Y.; Ren, F. Microstructure, mechanical properties, and sliding wear behavior of spark plasma sintered Ti-Cu alloys. *Metall. Mater. Trans. A* **2018**, *49*, 6147–6160. [CrossRef]
47. Sun, G.; Zhuang, S.; Jia, D.; Pan, X.; Sun, Y.; Tu, F.; Lu, M. Facile fabricating titanium/graphene composite with enhanced conductivity. *Mater. Lett.* **2023**, *333*, 133680. [CrossRef]

Disclaimer/Publisher's Note: The statements, opinions and data contained in all publications are solely those of the individual author(s) and contributor(s) and not of MDPI and/or the editor(s). MDPI and/or the editor(s) disclaim responsibility for any injury to people or property resulting from any ideas, methods, instructions or products referred to in the content.